polysaccharides

MDPI

Article

Physicochemical and Spectroscopic Characterization of Glycogen and Glycogen Phosphorylase *b* Complexes

Pandora Karakousi [1], Maria Karayianni [1,2,*], Evangelia D. Chrysina [1] and Stergios Pispas [2,*]

[1] Institute of Chemical Biology, National Hellenic Research Foundation, 48 Vassileos Constantinou Ave., 116 35 Athens, Greece; pkarakousi@eie.gr (P.K.); echrysina@eie.gr (E.D.C.)
[2] Theoretical and Physical Chemistry Institute, National Hellenic Research Foundation, 48 Vassileos Constantinou Ave., 116 35 Athens, Greece
* Correspondence: mkaragia@eie.gr (M.K.); pispas@eie.gr (S.P.)

Abstract: Glycogen is a natural polysaccharide used as an energy storage macromolecule. The role of glycogen metabolism in type 2 diabetes mellitus has been under investigation for several years, along with its implication in cancer and cardiovascular and neurodegenerative diseases. Previous studies using pig liver glycogen with rabbit muscle glycogen phosphorylase (RMGP*b*), which catalyzes the first step of glycogen degradation to glucose-1-phosphate, showed that the surface of an average glycogen molecule is covered by a total of 20 RMGP*b* dimeric molecules. In this work, we selected oyster glycogen (Glyc) to investigate its interaction with RMGP*b* by employing biophysical techniques. Dynamic, static, and electrophoretic light scattering were used to investigate the solution behaviors and structures of both the Glyc molecule itself and the formed complexes between Glyc and GP*b* at different mixing ratios. It was established that the interaction between oyster Glyc and RMGP*b* is similar to that previously reported for pig liver glycogen. Moreover, the structure of the complexed GP*b* was monitored by fluorescence and FTIR spectroscopy.

Keywords: glycogen; biopolymer; glycogen phosphorylase *b*; biophysical characterization; enzyme–biopolymer complexes

Citation: Karakousi, P.; Karayianni, M.; Chrysina, E.D.; Pispas, S. Physicochemical and Spectroscopic Characterization of Glycogen and Glycogen Phosphorylase *b* Complexes. *Polysaccharides* **2024**, *5*, 225–240. https://doi.org/10.3390/polysaccharides5030017

Academic Editor: Cong Wang

Received: 31 May 2024
Revised: 3 July 2024
Accepted: 4 July 2024
Published: 7 July 2024

1. Introduction

Glycogen is a branched polymer of glucose that humans and animals use as an energy reserve. In linear chains, glucose residues connect via α-1,4 glycosidic bonds, and in order to create branch points they connect via α-1,6 glycosidic ones. Glycogen branching is a key property of glycogen as it increases its solubility and allows it to become metabolized more quickly [1,2]. The role of glycogen in physiological processes has been investigated for a long time, and the literature on this research area is rather rich. However, it is only during recent years that the scientific community has started utilizing its properties as a material or nanomaterial for various applications, with a special focus towards nanomedicine [3]. The main reason for this is that there is an increasing interest in employing natural polysaccharides, including glycogen, as natural biomaterials due to their unique advantages of being biocompatible and biodegradable. Moreover, they can be chemically or biochemically modified to produce functional derivatives, which are important for various therapeutic applications [4,5]. Glycogen is rather attractive compared to other polysaccharides since it is not only biodegradable but also non-toxic. However, any chemical modification can lead to a cytotoxic and mutagenic reaction, which implies that glycogen nanoparticles require careful evaluation prior to their use [6].

The progress made so far in the development of glycogen as a functional advanced material is promising, but several key challenges need to be overcome. Studies on the in vivo fate of glycogen particles of different sizes, molecular weights, and surface functionalities, particularly with respect to the immune system and disease engagement, require further investigation [7]. With the aim of analyzing the chemistry of glycogen molecules,

it is essential to define molecular mass distributions, average chain lengths, and average branching frequencies. Important insights into the glycogen structure have emerged from the chemical analysis of mammalian glycogen, suggesting that a full-size glycogen molecule would consist of a total of ~55,000 glucose residues, a molecular mass of ~107 kDa, and a diameter of ~44 nm [8]. It is highly concentrated in the liver, although skeletal muscles contain the most glycogen by weight. It is also present in lower levels in other tissues, such as the kidney, heart, astrocytes, neurons, and brain. Importantly, glycogen serves to maintain glucose homeostasis in animal and human bodies. Because of this, its metabolism is primarily regulated by insulin and glucagon and other molecules in their downstream signaling pathways. Insulin and glucagon promote glycogen synthesis and breakdown, respectively. Many pathological conditions have been associated with different points of the glycogen metabolism pathway. Diseases involving enzymes that have important roles in glycogen synthesis, degradation, and/or regulation have significant adverse effects on the body [8,9]. Finding the links between glycogen metabolism and serious diseases, such as type 2 diabetes mellitus [10], cancer [11], and cardiovascular [12,13] and neurodegenerative diseases [14], remains a challenge for the scientific community.

The development of new research tools for integrated approaches currently allows for the systematic study of enzymes (molecular targets) involved in the metabolic pathway of glycogen biosynthesis and degradation in different tissues. Of the multitude of enzymes involved in this metabolic pathway, glycogen phosphorylase (GP, EC 2.4.1.1) plays a major role, catalyzing the first stage of its intracellular degradation to glucose 1-phosphate (Glc-1-P) and then to glucose [15,16]. GP is an allosteric enzyme which exists in at least two interconvertible forms, namely GP*b* (inactive, *T*-configuration) and GP*a* (active, *R*-configuration). Its distinct binding sites have been targeted for the development of new drugs using the structure-based drug design approach [17,18]. In the liver, the main mechanism controlling glycogenolysis is the phosphorylation of GP*b* → GP*a*, and according to previous studies, glucose inhibits the action of GP by synergistically acting with insulin to reduce degradation while increasing glycogen synthesis.

Previous studies using pig liver glycogen with rabbit muscle GP*b* (RMGP*b*) explored the complex formation between the two, and the kinetics of their interaction were monitored by the differences observed in the intensity of scattered light upon enzyme binding to glycogen. The equilibrium dissociation constants of the complexes and the adsorption capacity of glycogen were determined by sedimentation methods. The results show that the surface of an average glycogen molecule is covered by a total of 20 GP*b* dimeric molecules [19]. In this work, we investigate the solution properties of oyster Glyc and its complexation process with RMGP*b* as well as the biophysical properties of the formed complexes by means of dynamic, static, and electrophoretic light scattering (DLS, SLS, and ELS) techniques. Oyster Glyc was selected due to its high purity (<1% reducing sugars) and appropriateness for various applications concerning life sciences, biopharma, metabolomics, pharmaceuticals, etc. We present the interaction of the oyster Glyc-GP*b* system by focusing on the physicochemical properties and dynamic character of this interaction, paving the way for further studies involving natural polysaccharides as carriers. Furthermore, we report, for the first time, DLS measurements performed in "real-time" and during titration experiments, aiming to investigate the kinetics of the interaction between the two components, Glyc and GP*b*. Finally, spectroscopic methods like fluorescence spectroscopy (FS) and attenuated total reflection Fourier-transform infrared spectroscopy (ATR-FTIR) are also used to assess the tertiary and secondary structure, respectively, of the enzyme after complexation [20,21].

2. Materials and Methods

2.1. Materials

All chemicals were purchased from Sigma-Aldrich (Merck KGaA, Darmstadt, Germany). BES buffer (99.5%), sodium chloride (NaCl, 99%), hydrogen chloride solution (HCl, 37%), ethylenediaminetetraacetic acid tetrasodium salt dihydrate (EDTA 98.5%),

1,4-dithiothreitol (DTT), sodium azide (NaN_3, 99.5%), ethanol 100%, adenosine monophosphate (AMP), and toluene were used without any further purification.

2.2. Sample Preparation

Protein. RMGP*b* was isolated from rabbit skeletal muscle according to a variation in the protocol of the Fischer and Krebs method in which β-mercaptoethanol replaces L-cysteine in all purification steps [22]. The concentration of purified RMGP*b* was measured spectrophotometrically by the Beer–Lambert law using absorbance at 280 nm (the calculated molar absorption coefficient was 13.2 $(mg/mL)^{-1}$ cm^{-1} at 280 nm for a 1% wt. protein solution) [23]. RMGP*b* was dialyzed against BES buffer and was treated with charcoal to remove the remaining nucleotides and other impurities prior to complexation.

Glycogen. The preparation of glycogen from oyster (glycogen from oyster type II, Sigma-Aldrich G8751) also included treatment with charcoal to remove free glucose, residues containing glycans, and other biomolecules that react with the analytical reagents. The treated glycogen was then lyophilized and dialyzed against deionized water to a final concentration of 10% *w*/*v*. After treatment, the glycogen was stored at −19 °C prior to use. For the investigation of its solution properties, a 10 mg/mL stock solution was prepared by direct dissolution in water for injection (WFI) containing 200 ppm NaN_3 (so as to prevent bacterial growth). Subsequently, appropriate dilutions were performed in order to produce a range of solutions with concentrations of 1, 2.5, 5, and 7.5 mg/mL.

Preparation of Complex Solutions. The solution behaviors and structures of the formed complexes between oyster glycogen (Glyc) and GP*b* at different mixing ratios were investigated. All solutions were prepared using N,N-bis(2-hydroxyethyl)-2-amino ethanesulfonic acid buffer at pH 6.8 in the presence of 1 mM AMP. For the preparation of the different complex solutions, 1 mL of a 1 mg/mL Glyc solution was mixed with 0.1, 0.5, 1, 1.5, 2, 3, or 4 mL of a 1 mg/mL GP*b* solution, and then all solutions were diluted with BES buffer to a final volume of 5 mL. This way, the concentration of glycogen was kept constant at 0.2 mg/mL throughout the series of complex solutions, while that of the enzyme ranged from 0.02 to 0.8 mg/mL, thus changing the molar ratio of the two components. Moreover, the pH of the complex solutions was considered equal to that of the BES buffer (i.e., pH = 6.8). The corresponding mixing/molar ratios between glycogen and the enzyme for each complex solution are summarized in Table 1. All solutions were left to stand overnight for better equilibration.

Table 1. The compositions of the different Glyc + GP*b* complex solutions prepared for this study. The concentration of Glyc is equal to 0.2 mg/mL for all complex solutions.

Name	Enzyme Concentration C_{GPb} (mg/mL)	Total Complex Concentration C_{Tot} (mg/mL)	Enzyme/Glycogen Molar Ratio mol_{GPb}/mol_{Glyc}
Comp(1 + 0.1)	0.02	0.22	1.8
Comp(1 + 0.5)	0.1	0.3	9
Comp(1 + 1)	0.2	0.4	18
Comp(1 + 1.5)	0.3	0.5	27
Comp(1 + 2)	0.4	0.6	36
Comp(1 + 3)	0.6	0.8	54
Comp(1 + 4)	0.8	1	72

In order to investigate the kinetics of the complexation process between the two components, two different types of experiments were conducted. The first one involved the "real-time" measurement of the complex solution directly after mixing as a function of time, while the second one probed the complexation as a titration procedure, i.e., after consecutive additions of small aliquots of the enzyme solution to the glycogen one. More specifically, for the *real-time* experiment, 1 mL of a 1 mg/mL glycogen (Glyc) solution was mixed with 1 mL of an either 1.5 or 0.75 mg/mL RMGP*b* solution directly in the DLS glass

cell and then measured continuously every ~1 min for ~25 min. In a similar manner, for the *titration experiment*, in 1 mL of a 1 mg/mL glycogen (Glyc) solution, a total of 1 mL of an either 1.5 or 0.75 mg/mL GP*b* solution was added in aliquots of 100 μL (i.e., 10 additions in total) directly in the DLS glass cell, and the solution was left to equilibrate for 5 min after each addition before measurement. The concentration of the GP*b* enzyme, 1.5 or 0.75 mg/mL, was chosen so the molar ratio of the two components, mol_{GPb}/mol_{Glyc}, was equal to 27 or 13.5, respectively. All solutions were prepared with N,N-bis(2-hydroxyethyl)-2-amino ethanesulfonic acid BES buffer (10 mM BES, 0.1 mM EDTA, 0.5 mM DTT, 0.01% NaN_3) at pH 6.8 in the presence of 1 mM AMP.

2.3. Methods

Dynamic and Static Light Scattering (DLS and SLS). DLS measurements were performed on an ALV/CGS-3 compact goniometer system (ALVGmbH, Hessen, Germany) equipped with an ALV-5000/EPP multi-tau digital correlator, a He-Ne laser (λ = 632.8 nm), and an avalanche photodiode detector. All sample solutions were filtered through 0.45 μm hydrophilic PVDF syringe filters before measurement to remove any dust particles or large aggregates. The samples were loaded into standard soda–lime glass dust-free cylindrical cells that were 1 cm width, and measurements were performed at a series of angles in the range of 45–135°.

Scattered light intensity autocorrelation functions $g_2(\tau)$ and field autocorrelation functions $g_1(\tau)$ were connected via Siegert relation using Equation (1):

$$g_2(\tau) - 1 = \beta|g_1(\tau)| \quad (1)$$

where β is a normalization constant and τ is the lag time.

The characteristic relaxation time $\tau_{rel}(q)$, which was obtained by the CONTIN analysis, can lead to the characteristic relaxation rate $\Gamma(q)$ via Equation (2), which leads to the diffusion coefficient D via Equation (3).

$$\Gamma(q) = 1/\tau_{rel}(q) \quad (2)$$

$$\Gamma = Dq^2 \quad (3)$$

Using the Stokes–Einstein equation [24], parameters such as the hydrodynamic radius (R_h) of the particles under study can be calculated as shown in Equation (4):

$$R_h = k_B T/6\pi\eta D_T \quad (4)$$

where k_B is the Boltzmann constant, η the solution's viscosity, and D_T is the translational diffusion coefficient [25,26].

It should be noted that for the measured scattered intensity values, there is a standard deviation of approximately 1–2%, while for the calculated R_h values, the corresponding standard deviation is about 5%.

Multiangle static light scattering (SLS) measurements were obtained by the Zimm method using Equation (5):

$$\frac{Kc}{R_\theta} = \frac{1}{M_w}\left(1 + \frac{1}{3}R_g^2 q^2\right) + 2A_2 c \quad (5)$$

where M_w is the weight-averaged molecular weight, R_g is the average radius of gyration, A_2 is the second osmotic virial coefficient, c is the Glyc solution concentration, and R_θ is the corrected Rayleigh ratio (which depends on the concentration c and the magnitude of the scattering vector q), and the constant factor K is given by the following relationship:

$$K = \frac{4\pi^2 n_0^2}{\Lambda_0^4 N_A}\left(\frac{dn}{dc}\right)^2 \quad (6)$$

where n_0, λ_0, N_A, and dn/dc are the refractive index of the solvent, the laser wavelength in vacuum, Avogadro's number, and the refractive index increment of Glyc with respect to the solvent, respectively. For the refractive index increment of the Glyc solutions in WFI, a value of 0.151 mL/g was used according to previous studies [27,28].

Electrophoretic Light Scattering (ELS). Zeta potential (ζ_P) measurements were obtained with a Zetasizer Nano-ZS (Malvern Panalytical Ltd., Malvern, United Kingdom) equipped with a He-Ne laser (λ = 633 nm) and an avalanche photodiode detector. The Henry equation in the Smoluchowski approximation was used for the zeta potential calculation. ζ_P values were determined using the Smoluchowski equation $\zeta_P = 4\pi\eta\nu/\varepsilon$, where η is the solvent viscosity, ν is the electrophoretic mobility, and ε is the dielectric constant of the solvent, and they are reported as averages of fifty repeated measurements at a 173° scattering angle and at room temperature.

Fourier-Transform Infrared Spectroscopy (FTIR). A mid-infrared FTIR spectrometer (Equinox 55 by Bruker GmbH, Ettlingen, Germany) equipped with an attenuated total reflectance (ATR) accessory (DuraSamplIR II by SensIR Technologies, Danbury, CT, USA) with a spectral range of 5000–550 cm^{-1} was used. Background spectra were obtained by recording the pristine and desiccated ATR diamond crystal surface in ambient air. The measurements of the complex solutions were performed in the dry state, by creating a thin film of the solution's components on the ATR diamond crystal, after solvent evaporation in a stream of nitrogen. Specifically, a small aliquot of each solution was placed on the ATR element and dried under a N_2 flow before measurement. For each sample, the final spectrum is the average of three 100-scan measurements at a 2 cm^{-1} resolution. The measurement of each sample was bracketed by two background spectra to allow for the elimination of H_2O vapor bands by interpolation. Moreover, the spectral contribution of the specific buffer used for the preparation of the complex solutions (BES buffer with 1 mM AMP) was suitably subtracted from the final spectra.

Fluorescence Spectroscopy. Fluorescence arises from a three-stage process occurring in specific molecules, typically polyaromatic hydrocarbons or heterocycles, referred to as fluorophores or fluorescent dyes. A fluorescent probe is a specially designed fluorophore that reacts to a specific stimulus or targets a particular region within a biological specimen [29]. The steady-state fluorescence spectra of the tryptophan residues of the neat and complexed RMGP*b* were recorded with a double-grating excitation and a single-grating emission spectrofluorometer (Fluorolog-3, model FL3-21, Jobin Yvon-Spex, Horiba Ltd., Kyoto, Japan) at room temperature. The excitation wavelength used was λ = 295 nm, and the emission spectra were recorded in the region of 315–500 nm, with an increment of 1 nm, using an integration time of 0.5 s. Slit openings of 1 nm were used for both the excitation and the emitted beam. Under the employed experimental conditions, fluorescence from the tryptophan residues of GP*b* was observed and utilized to extract information about the conformation of the enzyme, while the free glycogen solutions did not show any fluorescence.

3. Results

3.1. Glycogen Solution Properties

Initially, we investigated the solution properties of pure Glyc by performing DLS and multiangle SLS measurements of different Glyc solutions in water (specifically WFI with 200 ppm NaN_3) at concentrations in the range of 1 to 10 mg/mL. The obtained results in regard to the values of the scattered intensity at 90°, I_{90}, as a function of the glycogen concentration, the corresponding size distribution functions, and the constructed Zimm plot are presented in Figure 1. The values for the parameters derived from the multiangle SLS measurements, that is, the weight-averaged molecular weight, M_w; the radius of gyration, Rg; and the second osmotic virial coefficient, A_2, are summarized in Table 2. Also included in Table 2 are the values for the corresponding average hydrodynamic radius, R_h, derived from the simultaneous dynamic measurements (i.e., independent of the concentration and scattering angle) and the characteristic ratio $\rho = R_g/R_h$, which

provides valuable information relative to the shape, density, and overall conformation of the scattering species in the solution.

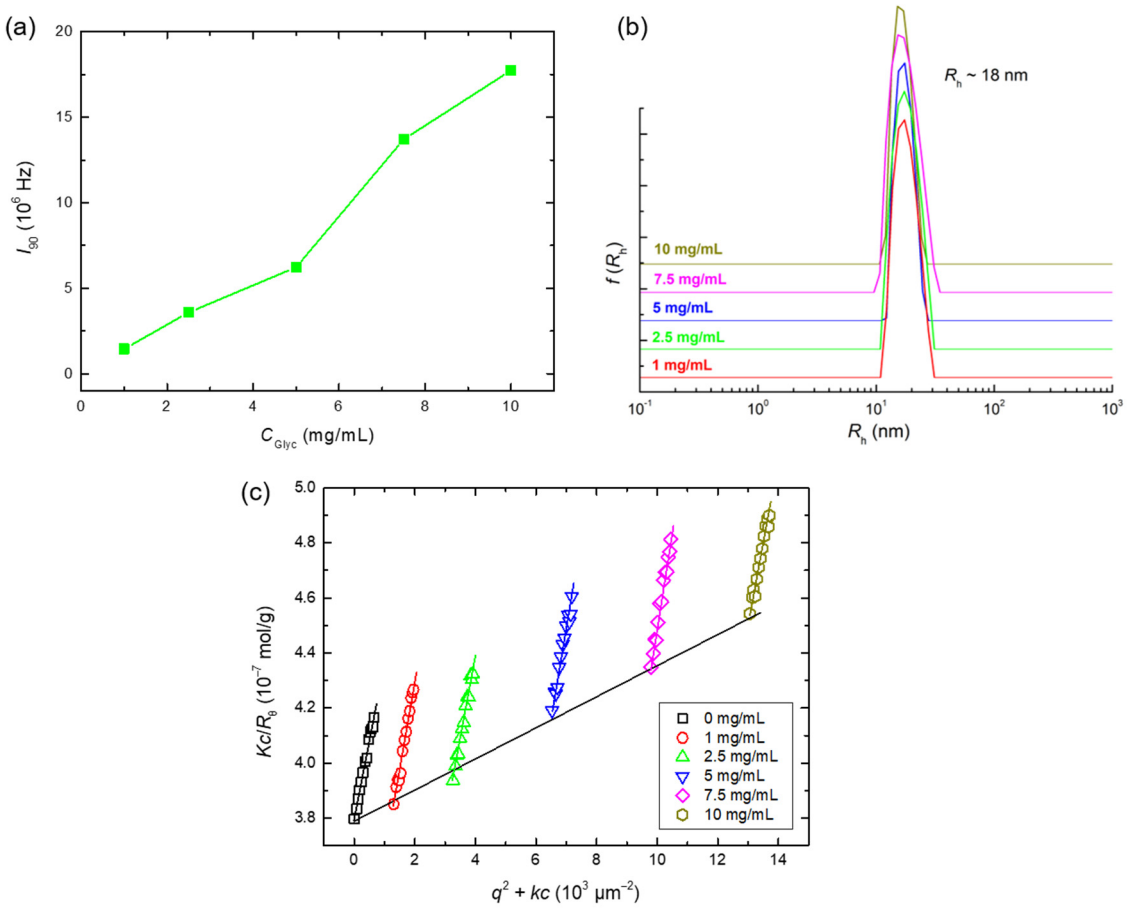

Figure 1. Light scattering results: (**a**) DLS scattered intensity values at 90°, I_{90}, as function of Glyc concentration, (**b**) DLS size distribution functions (SDFs) obtained at 90°, and (**c**) multiangle SLS Zimm plot for pure Glyc solutions in WFI at different concentrations ranging from 1 to 10 mg/mL.

Table 2. Summary of multiangle static and dynamic light scattering results for pure Glyc.

M_w (10^6 g/mol)	R_g (nm)	R_h (nm)	$\rho = R_g/R_h$	A_2 (10^{-6} mol mL/g^2)
2.6	21.7	17.7	1.23	4.5

Approximate standard deviations: M_w, 5%; R_g, 13%; R_h, 17%; A_2, 26%.

As it can be seen, Figure 1a verifies the expected linear dependency between the I_{90} values and the concentration of the solution since the scattered intensity is proportional to the total mass of the scattering species/molecules in the solution. The corresponding SDFs shown in Figure 1b are almost identical for all different concentrations measured and reveal the presence of only one narrow peak at R_h values of about 18 nm, a size which is similar to the previously reported experimental findings concerning oyster glycogen [30–33]. Moreover, no signs of aggregation between the Glyc molecules are evidenced since no additional peaks at higher R_h values are discerned even at higher concentrations. As far as the SLS results are concerned, the calculated molecular weight for the specific Glyc sample is equal to 2.6×10^6 g/mol, which corresponds to an approximate number of 14,400 glucose units. This M_w value is somewhat lower than the ones found in the literature for oyster glycogen [31,32,34–36], which are in the range of 5 to 7×10^6 g/mol. This fact could be correlated to the particular cleaning protocol/charcoal treatment implemented in this study.

Regarding the size and shape of the Glyc molecule, the calculated R_g and R_h values are 21.7 and 17.7 nm, respectively, corresponding to a ρ ratio equal to 1.23, which coincides with the 1.225 theoretically predicted ρ value for hyperbranched structures [27,35]. Finally, the second virial coefficient A_2 exhibits a molecular weight dependence expressed by a scaling law of the form $A_2 \propto M_w^{a_{A_2}}$, which, in this case, results in an a_{A_2} exponent value equal to −0.83, which is also indicative of hyperbranched spherical architectures [27,35].

3.2. Glycogen–Glycogen Phosphorylase Complexation

The formation of glycogen/enzyme complexes through electrostatic complexation were explored by dynamic light scattering measurements (DLS). The properties of the stable complex solutions were initially examined by DLS measurements, and Figure 2 shows the obtained scattered intensity values derived from measurements at 90°, I_{90}; as a function of the GP*b* concentration, C_{GPb}; or the enzyme-to-glycogen molar ratio, mol_{GPb}/mol_{Glyc}. More specifically, Figure 2 includes both the actual intensity values obtained from the measurement of each complex solution sample (i.e., as measured) as well as the corrected intensity values derived from the measured ones after subtracting the corresponding contributions of glycogen and the enzyme according to their relative concentration. Note that the I_{90} value at C_{GPb} = 0 for the as-measured data (i.e., square symbols in Figure 2) corresponds to that of a free glycogen solution at the same concentration as in the complexes (C_{Glyc} = 0.2 mg/mL). The observed gradual increase in I_{90} values, which is also evident after the correction for the contribution of the constituents, serves as a direct proof of complexation and complex formation since the scattered intensity is proportional to the mass of the scattering species in the solution.

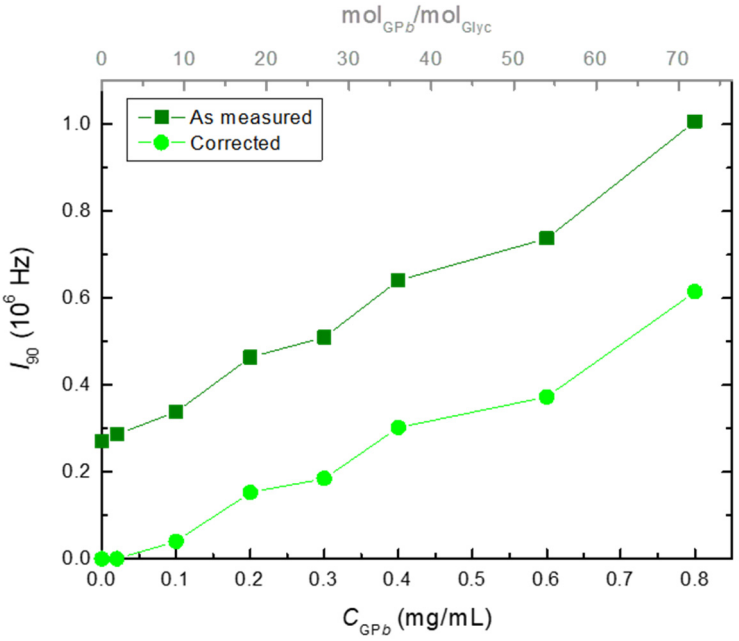

Figure 2. The DLS scattered intensity at 90°, I_{90}, as measured values for the Glyc + GP*b* complex solutions as a function of C_{GPb} or mol_{GPb}/mol_{Glyc}. Also included for comparison are the corrected I_{90} values after the subtraction of the corresponding contribution of the free glycogen and enzyme constituents.

Regarding the corresponding sizes, the solutions of the complexes exhibit one main peak in all cases with R_h values of about 18 nm, as observed in the obtained size distribution functions shown in Figure 3. Note that the free glycogen solution also exhibits a similar peak around 18 nm, as also seen in Figure 1b. As the concentration of phosphorylase increases, a broadening of the main peak of the complex solutions can be observed, but the mean size remains practically the same. One possible explanation for this observation is that

the size of the complexes is mostly determined by the size of the glycogen molecules. This may further indicate that glycogen molecules may be deformed to some extent and engulf the enzyme molecules upon interaction. Quite interestingly, for complex solutions with $C_{GPb} \geq 0.2$ mg/mL, a second small peak with a size of about 3.5 nm is observed. This peak apparently indicates the presence of uncomplexed phosphorylase in the corresponding solutions of the complexes, thus suggesting that the interaction capacity between the two components is rather limited. In other words, each glycogen molecule can bind a specific finite number of phosphorylase enzyme molecules, and as the enzyme concentration increases, an excess of GP*b* molecules is observed. At the same time, the contribution of the GP*b* peak at 3.5 nm to the overall distribution seems to increase for C_{GPb} values up to 0.4 mg/mL, providing evidence for the increase in uncomplexed GP*b* (Figure 3b), while for higher C_{GPb} values ($\geq$ 0.6 mg/mL), no significant changes are observed. This increase in the uncomplexed GP*b* at higher enzyme concentrations or equivalent molar ratios could be an indication that the maximum interaction capacity between the two components was reached for $mol_{GPb}/mol_{Glyc} \geq 36$.

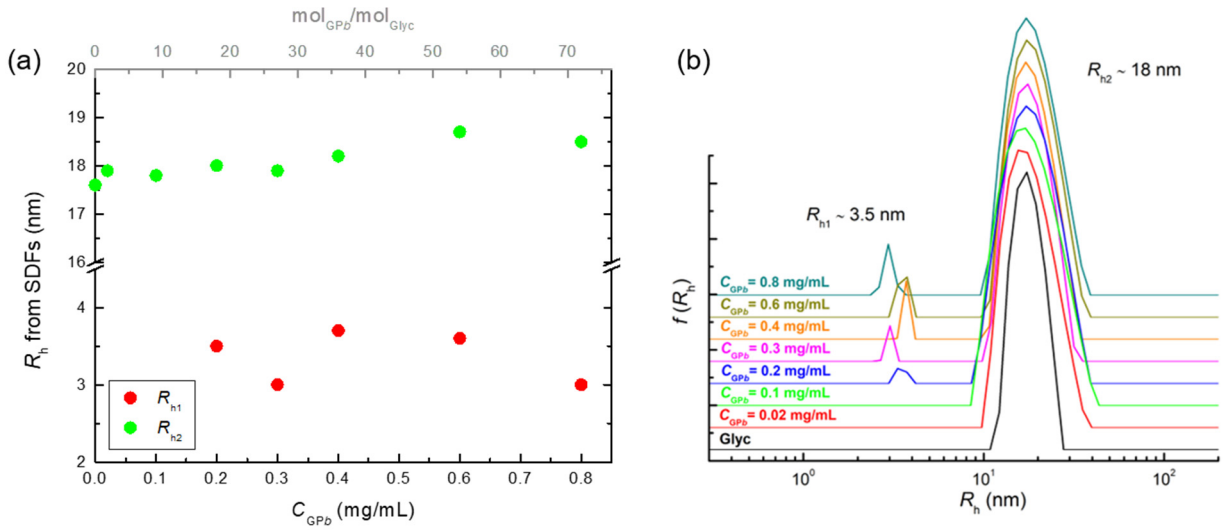

Figure 3. (**a**) Hydrodynamic radius, R_h, values as functions of C_{GPb} or mol_{GPb}/mol_{Glyc} derived from (**b**) the DLS size distribution functions (SDFs) obtained at 90° for the Glyc + GP*b* complex solutions. The corresponding SDF of free glycogen is also included for comparison.

Another physicochemical characteristic of the formed complexes is their effective charge, which was acquired via electrophoretic light scattering (ELS) measurements, yielding the zeta potential ζ_P values presented in Figure 4 in an identical manner to the previous DLS results. The observed decrease in the absolute value of the zeta potential as the concentration of the enzyme becomes higher is an indication of the charge neutralization that occurs due to complexation. Moreover, for $C_{GPb} \geq 0.4$ mg/mL (or $mol_{GPb}/mol_{Glyc} \geq 36$), the zeta potential of the complexes seems to reach a plateau value, similar to that of neat GP*b*, which was measured at about -12 ± 5 mV. According to these observations, the proposed scenario is that each spherical glycogen molecule binds in its periphery many GP*b* molecules, resulting in complexes that can be described as glycogen molecules externally decorated with several phosphorylases.

3.3. Glycogen–Glycogen Phosphorylase Complexation Kinetics

In an attempt to examine, in more detail, the kinetics of the complexation process between glycogen and glycogen phosphorylase, two different types of time-dependent measurements/experiments were designed and executed. Firstly, a *real-time* measurement was carried out in which the two components (Glyc and GP*b*) were mixed directly in the DLS cell followed by consecutive measurements (at a 90° angle) as a function of time. The

second type of experiment was performed in a *titration* manner, meaning that small aliquots of the GP*b* solution were gradually added to that of Glyc, once again directly in the DLS cell, and after 5 min of equilibration, the measurement for each addition was performed. For both set-ups, 1 mL of a 1 mg/mL Glyc solution was initially placed in the DLS cell, and a total of 1 mL of a 0.75 or 1.5 mg/mL GP*b* solution was subsequently added either directly (*real time* experiment) or in 100 μL aliquots (*titration* experiment). The two different concentrations of the enzyme correspond to a molar ratio (mol_{GPb}/mol_{Glyc}) of 13.5 or 27, which are both below the limit of the maximum interaction capacity, as established from the previously obtained results for the complexes.

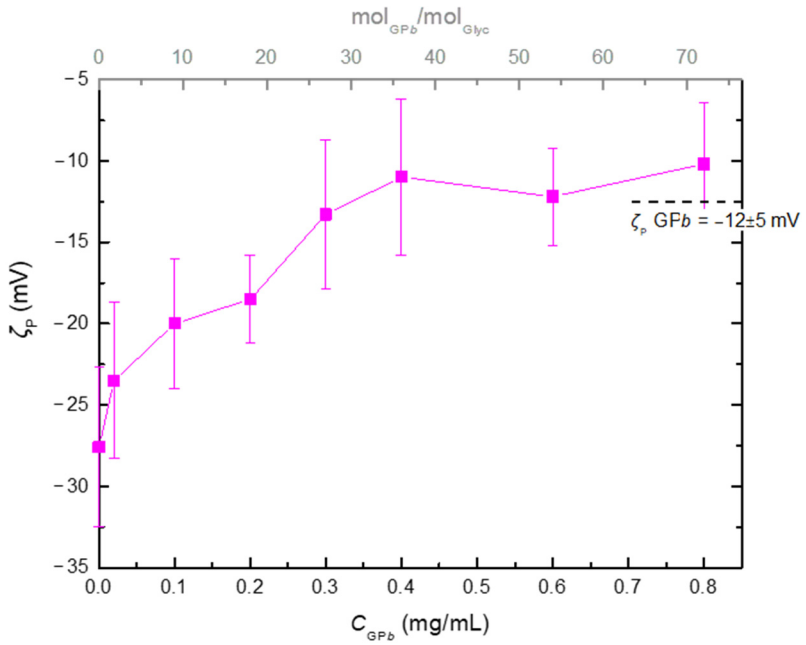

Figure 4. The ELS zeta potential, ζ_P, values for the Glyc + GP*b* complex solutions as functions of C_{GPb} or mol_{GPb}/mol_{Glyc}. The corresponding ζ_P value for neat GPb is also noted (dashed line) for comparison.

For the *real-time* experiment, the measured I_{90} values (corrected for the contribution of the constituents) for the two different mol_{GPb}/mol_{Glyc} ratios are presented in Figure 5a as a function of time. As it can be seen, although there are some fluctuations, the scattered intensity values or, equivalently, the mass of the complexes remains practically constant throughout the entire timescale of the measurement. Apparently, the complexation process between Glyc and GP*b* molecules occurs too fast to be detected under specific experimental conditions. Nevertheless, it is worth noting that the overall intensity values are higher for $mol_{GPb}/mol_{Glyc} = 27$, thus verifying the increase in the mass of the complexes as the enzyme content increases, which is in accordance with the previous results. The same observation also stands for the corresponding sizes of the complexes, as evidenced from the R_h values shown in Figure 5b derived from the corresponding size distribution functions (shown in Figure S1). For both molar ratios, no significant changes are observed in the size of both peaks, while the main peak (R_{h2}) which indicates the size of the complexes seems somewhat larger overall (about 20 nm) at $mol_{GPb}/mol_{Glyc} = 27$ than at $mol_{GPb}/mol_{Glyc} = 13.5$ (about 18 nm). This finding is in accordance with the notion that at higher molar ratios, each glycogen molecule interacts with a larger number of phosphorylases.

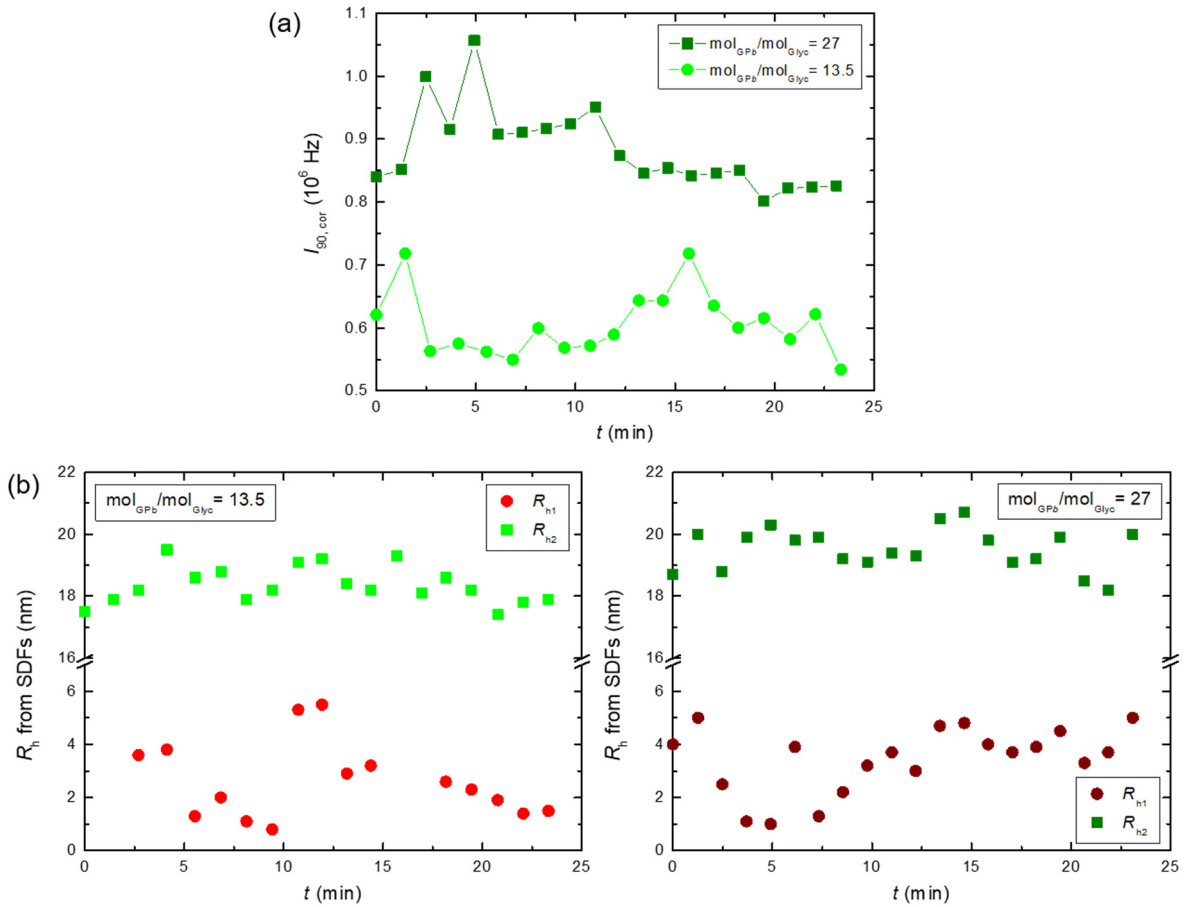

Figure 5. *Real-time* experiment results: (**a**) scattered intensity values at 90°, I_{90}, and (**b**) hydrodynamic radius, R_h, values derived from the corresponding size distribution functions (SDFs) obtained at 90° as a function of time for two different molar ratio values, mol_{GPb}/mol_{Glyc} = 13.5 or 27.

Since the *real-time* monitoring of the kinetics of the complexation process proved to be unattainable, a *titration* experiment was conceptualized, aiming to determine whether the decrease in the number of phosphorylase molecules interacting with glycogen would affect their complexation. In this case, the experimental procedure involved the addition of small aliquots (100 µL) of the GP*b* solution into the DLS cell that contained the Glyc solution, as described above, and the measurement was performed five minutes after each addition of the enzyme to ensure the equilibration of the system. The same concentration of the phosphorylase solution was used, either 0.75 or 1.5 mg/mL, so the final (after the addition of the whole 1 mL of the enzyme solution) molar ratio corresponded to mol_{GPb}/mol_{Glyc} = 13.5 or 27. Figure 6 presents the results of this measurement with regard to the corrected I_{90} values, along with the R_h values derived from the corresponding size distribution functions (shown in Figure S2), as a function of the mol_{GPb}/mol_{Glyc} molar ratio for the two different values of C_{GPb} used. As it can be observed, the mass was mainly larger (I_{90} values), and to a lesser extent, the size (R_{h2} values) of the complexes formed at higher C_{GPb} values but with the same molar ratio. As it can be observed, the mass (I_{90} values) of the complexes formed at higher C_{GPb} values but with the same molar ratio is larger, although their corresponding sizes (R_{h2} values) are similar. This observation is directly correlated to the interaction degree between Glyc and GP*b* molecules in the sense that when the concentration of GP*b* is higher, each Glyc interacts with a higher number of enzyme molecules, thus forming complexes with an increased mass, although the molar ratio between the two components is the same. One logical explanation for this finding is that after the Glyc molecule has interacted with a number of GP*b* molecules, its ability to further bind additional ones is significantly hindered, most probably due to

conformational restrictions. In other words, it is difficult for an already formed Glyc + GP*b* complex to accommodate additional enzyme molecules, and this affects the structure of the resulting complexes. Therefore, the complexes formed at C_{GPb} = 0.75 mg/mL and the same mol_{GPb}/mol_{Glyc} value have a lower mass than the ones at a higher C_{GPb} since they correspond to double the number of titrations. At the same time, the size of the complexes is mostly determined by the size of the Glyc molecule and therefore does not show significant differences independently of the number of phosphorylases bound per glycogen. One final remark here is the presence of free/unbound GP*b* (R_{h1} peak), which is barely discerned at lower concentrations of the enzyme (see Figure S2).

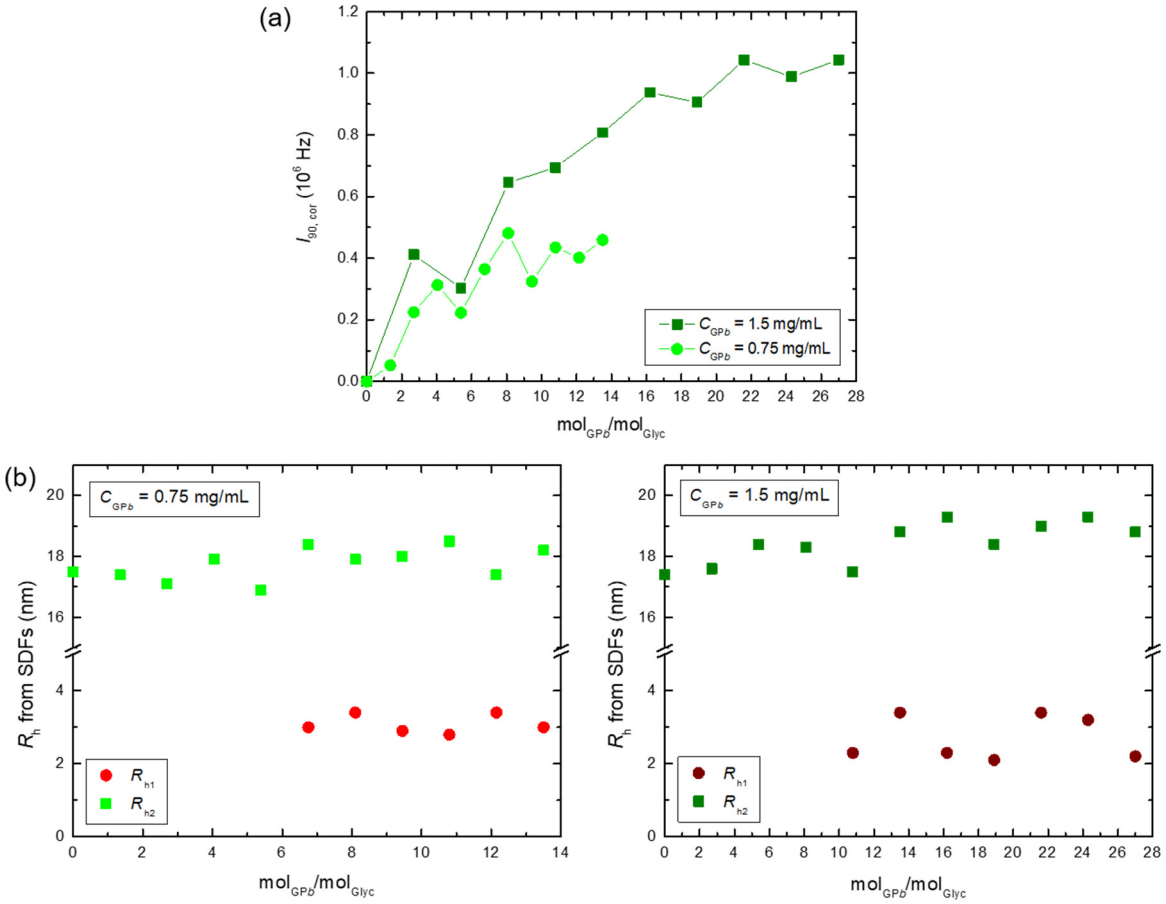

Figure 6. The *titration* experiment results: (**a**) the scattered intensity values at 90°, I_{90}, and (**b**) hydrodynamic radius, R_h, values derived from the corresponding size distribution functions (SDFs) obtained at 90° as a function of mol_{GPb}/mol_{Glyc} for two different GP*b* concentration values, C_{GPb} = 0.75 or 1.5 mg/mL.

3.4. The Enzyme Structure within the Complexes

The structure of a protein/enzyme and its configuration in space are the main properties that determine its function. For this reason, in most biochemical and biotechnological applications where proteins are involved, the control of structural conservation is of paramount importance. Therefore, it is necessary to investigate the overall structure of glycogen phosphorylase in the complexes using fluorescence and mid-infrared spectroscopic techniques, which detect the tertiary and secondary structures of the enzyme molecule, respectively.

Amongst the three fluorescent amino acid constituents of proteins, tryptophane (Trp) is the most abundant. The photophysical properties of Trp are highly sensitive to its local environment; thus, the corresponding emission spectrum can provide very important information about changes in the polarity of the surroundings of Trp residues and, accordingly,

in the structure of the whole protein molecule. The other two amino acids are phenylalanine (Phe) and tyrosine (Tyr), with the first one having very low intrinsic fluorescence, while the emission of the second one is often quenched in native proteins, probably due to its interaction with the peptide chain or through energy transfer to Trp [37].

The tryptophane emission spectra (excitation at 295 nm) of the solutions of the Glyc + GP*b* complexes were recorded to probe the structure of the complexed enzyme. The resulting spectra are shown in Figure 7, where the corresponding spectrum of free/uncomplexed GP*b*, along with that of free glycogen (which confirms the absence of fluorescence) are also included for comparison. All spectra exhibit the characteristic peak of tryptophane with a maximum at about 350 nm, while the intensity of the peak is directly proportional to the concentration of GP*b* in the solution (for this reason, the fluorescence spectra of the solutions of the complexes at C_{GPb} = 0.4 and 0.1 mg/mL are directly compared with the corresponding spectra of neat GP*b* at concentrations of 0.5 and 0.1 mg/mL, as shown in Figure S3). Since there are no significant changes in the tryptophane peak position for the complexed enzyme, it can be concluded that GP*b* is not subjected to substantial conformational changes when it interacts with glycogen.

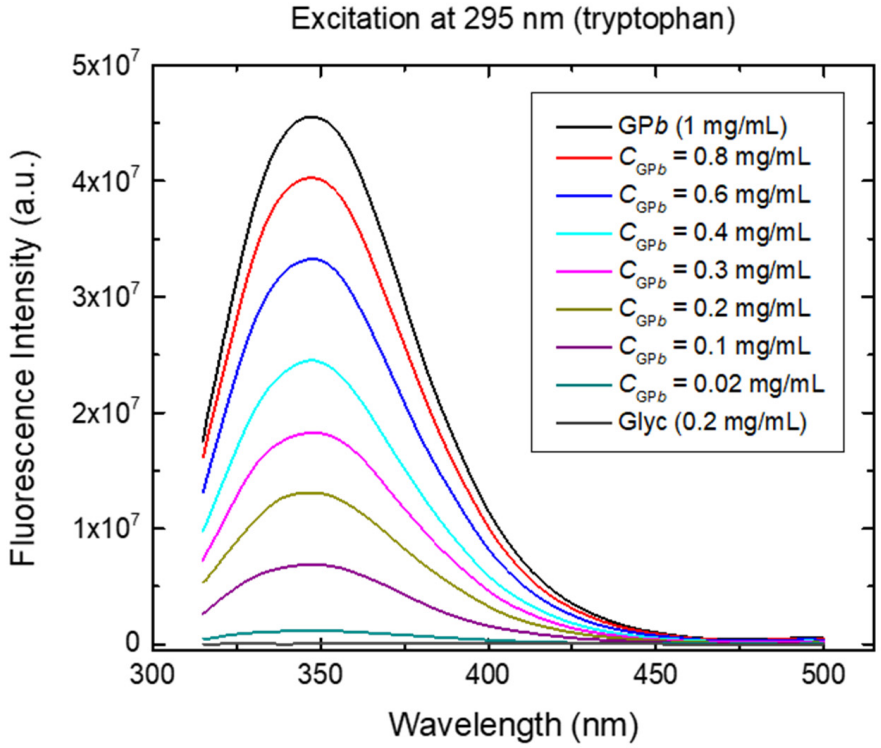

Figure 7. Fluorescence spectra obtained using tryptophan excitation at 295 nm of Glyc + GP*b* complex solutions. Corresponding spectrum of neat phosphorylase at 1 mg/mL concentration, as well as that of glycogen at 0.2 mg/mL concentration, are also included for comparison.

Additionally, infrared (IR) spectroscopy measurements were performed for the determination of the secondary structure of the complexed enzyme. Figure 8 presents the obtained FTIR-ATR spectra of the Glyc + GP*b* complexes, together with the corresponding spectra of the neat enzyme and glycogen for comparison, in the Amide I and II regions. These peaks mainly represent the vibrational profile of the peptide bond and are characteristic of protein/enzyme samples. As it can be seen, the overall spectral profile (i.e., the maximum position and shape) of both Amide bands is clearly preserved in the complexes with $C_{GPb} \geq 0.2$ mg/mL, indicating the absence of significant configurational changes [38,39]. For the complex solutions at lower C_{GPb} values (i.e., 0.02 and 0.1 mg/mL), both Amide bands are not so well discerned due to the low concentration of the enzyme and the contribution of the spectral characteristics of both Glyc and the used buffer (although its

contribution has been subtracted from the spectra, as shown in Figure 8). Nevertheless, no significant spectral shifts that would denote the denaturation of the enzyme are observed. Thus, the results obtained from the FTIR-ATR technique also confirm that the enzyme maintains its native conformation upon complexation.

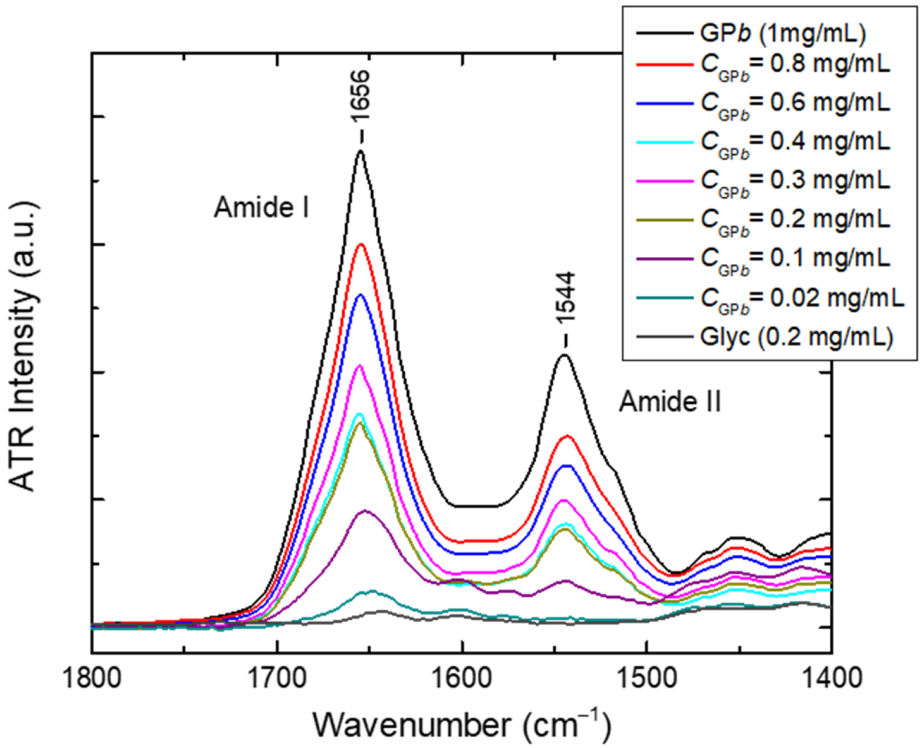

Figure 8. The FTIR-ATR spectra in the Amide I and II regions of the Glyc + GP*b* complex solutions. The corresponding spectrum of neat phosphorylase at a 1 mg/mL concentration, as well as that of glycogen at a 0.2 mg/mL concentration, are also included for comparison.

4. Conclusions

The aim of the present study was to investigate the solution properties of oyster glycogen (Glyc) and its interaction with rabbit muscle glycogen phosphorylase *b* (GP*b*) by means of light scattering techniques, since the specific system has not yet been examined from a physicochemical point of view. Overall, the results obtained confirm the known structural characteristics of the Glyc molecule, as well as the fact that oyster glycogen interacts with GP*b* in a similar way to that of pig liver glycogen, as previously reported in the literature [19]. More specifically, the light scattering results confirm the hyperbranched spherical architecture of Glyc while proving that the complexation between Glyc and GP*b* takes place, although the apparent mass and size of the formed complexes are only slightly higher than the corresponding ones of Glyc. The observed increase in the uncomplexed GP*b* at a higher molar ratio suggests that a maximum interaction capacity between the two components was reached for $mol_{GPb}/mol_{Glyc} \geq 36$. This finding is in good agreement with the corresponding total interaction capacity of 20 GP*b* dimeric molecules covering each pig liver Glyc [19], demonstrating the similarities between the two Glyc-GP*b* systems. Moreover, the negative effective charge of the complexes decreases as a function of the GP*b* concentration, reaching values closer to that of the pure enzyme, indicating that the resulting complexes can be described as glycogen molecules decorated with several phosphorylases. Additionally, the fluorescence and infrared spectroscopic investigation confirmed that the structure of the enzyme remains stable even after complexation. Finally, the recording of the kinetics of the complexation process proved to be unfeasible via *real-time* DLS measurements, most probably because it is too fast, while it was also established that the mixing protocol of the two components (i.e., direct mixing or titration)

affects the structure of the resulting complexes. As a closing remark, we hope that the different experimental measuring protocols in regard to light scattering techniques applied in the course of this study showcase the importance of these methods in the investigation of biological interactions in similar macromolecular systems, as well as the plethora of potentially attainable information.

Supplementary Materials: The following supporting information can be downloaded at https://www.mdpi.com/article/10.3390/polysaccharides5030017/s1, Figure S1: The *real-time* experiment DLS size distribution functions (SDFs) obtained at 90°, as a function of time for two different molar ratio values, mol_{GPb}/mol_{Glyc} = 13.5 and 27. Note that the GP*b* peak is more pronounced at a higher molar ratio (double GP*b* concentration); Figure S2: The *titration* experiment DLS size distribution functions (SDFs) obtained at 90° as function of mol_{GPb}/mol_{Glyc} for two different GP*b* concentration values, C_{GPb} = 0.75 or 1.5 mg/mL; Figure S3: A comparison of the fluorescence spectra of the solutions of the complexes at C_{GPb} = 0.4 and 0.1 mg/mL, with the corresponding spectra of neat GP*b* at concentrations of 0.5 and 0.1 mg/mL (the legends indicate the series of the spectra from top to bottom).

Author Contributions: Conceptualization, S.P., M.K. and E.D.C.; methodology, S.P., M.K. and E.D.C.; formal analysis, P.K. and M.K.; investigation, P.K. and M.K.; data curation, P.K. and M.K.; writing—original draft preparation, P.K. and M.K.; writing—review and editing, M.K., S.P. and E.D.C.; supervision, S.P. and E.D.C.; funding acquisition, P.K. and E.D.C. All authors have read and agreed to the published version of the manuscript.

Funding: The implementation of the present work is part of Pandora Karakousi's doctoral thesis and has been co-financed by Greece and the European Union (European Social Fund-ESF) through the Operational Programme "Human Resources Development, Education and Lifelong Learning" in the context of the act titled "Enhancing Human Resources Research Potential by undertaking a Doctoral Research" Sub-action 2: IKY Scholarship Programme for PhD candidates in the Greek Universities. We also acknowledge the support of this work that was provided by Instruct-hub in NHRF by the project "INSPIRED" (MIS 5002550) under the action "Reinforcement of the Research and Innovation Infrastructure", funded by the Operational Programme "Competitiveness, Entrepreneurship and Innovation" (NSRF 2014–2020).

Institutional Review Board Statement: Not applicable.

Data Availability Statement: Data are contained within the article and Supplementary Materials.

Conflicts of Interest: The authors declare no conflicts of interest.

References

1. Melendez-Hevia, E.; Waddell, T.G.; Shelton, E.D. Optimization of Molecular Design in the Evolution of Metabolism: The Glycogen Molecule. *Biochem. J.* **1993**, *295*, 477–483. [CrossRef] [PubMed]
2. Meléndez, R.; Meléndez-Hevia, E.; Cascante, M. How Did Glycogen Structure Evolve to Satisfy the Requirement for Rapid Mobilization of Glucose? A Problem of Physical Constraints in Structure Building. *J. Mol. Evol.* **1997**, *45*, 446–455. [CrossRef] [PubMed]
3. Besford, Q.A. The Sweetest Polymer Nanoparticles: Opportunities Ahead for Glycogen in Nanomedicine. *Soft Matter* **2024**, *20*, 3577–3584. [CrossRef] [PubMed]
4. Daghlas, S.A.; Mohiuddin, S.S. Biochemistry, Glycogen. 2023 May 1. In *StatPearls [Internet]*; StatPearls Publishing: Treasure Island, FL, USA, 2024.
5. García-González, C.A.; Alnaief, M.; Smirnova, I. Polysaccharide-Based Aerogels—Promising Biodegradable Carriers for Drug Delivery Systems. *Carbohydr. Polym.* **2011**, *86*, 1425–1438. [CrossRef]
6. Gurcan, C.; Taheri, H.; Bianco, A.; Delogu, L.G.; Yilmazer, A. A Closer Look at the Genotoxicity of Graphene Based Materials. *J. Phys. Mater.* **2020**, *3*, 014007. [CrossRef]
7. Besford, Q.A.; Cavalieri, F.; Caruso, F. Glycogen as a Building Block for Advanced Biological Materials. *Adv. Mater.* **2020**, *32*, 1904625. [CrossRef] [PubMed]
8. Roach, P.J.; Depaoli-Roach, A.A.; Hurley, T.D.; Tagliabracci, V.S. Glycogen and Its Metabolism: Some New Developments and Old Themes. *Biochem. J.* **2012**, *441*, 763–787. [CrossRef] [PubMed]
9. Adeva-Andany, M.M.; González-Lucán, M.; Donapetry-García, C.; Fernández-Fernández, C.; Ameneiros-Rodríguez, E. Glycogen Metabolism in Humans. *BBA Clin.* **2016**, *5*, 85–100. [CrossRef]
10. Treadway, J.L.; Mendys, P.; Hoover, D.J. Glycogen Phosphorylase Inhibitors for Treatment of Type 2 Diabetes Mellitus. *Expert Opin. Investig. Drugs* **2001**, *10*, 439–454. [CrossRef]

11. Zois, C.E.; Harris, A.L. Glycogen Metabolism Has a Key Role in the Cancer Microenvironment and Provides New Targets for Cancer Therapy. *J. Mol. Med.* **2016**, *94*, 137–154. [CrossRef]
12. Aydin, S.; Ugur, K.; Aydin, S.; Sahin, İ.; Yardim, M. Biomarkers in Acute Myocardial Infarction: Current Perspectives. *Vasc. Health Risk Manag.* **2019**, *15*, 1–10. [CrossRef] [PubMed]
13. Mair, J. Glycogen Phosphorylase Isoenzyme BB to Diagnose Ischaemic Myocardial Damage. *Clin. Chim. Acta* **1998**, *272*, 79–86. [CrossRef] [PubMed]
14. Falkowska, A.; Gutowska, I.; Goschorska, M.; Nowacki, P.; Chlubek, D.; Baranowska-Bosiacka, I. Energy Metabolism of the Brain, Including the Cooperation between Astrocytes and Neurons, Especially in the Context of Glycogen Metabolism. *Int. J. Mol. Sci.* **2015**, *16*, 25959–25981. [CrossRef]
15. Newgard, C.B.; Hwang, P.K.; Fletterick, R.J. The Family of Glycogen Phosphorylases: Structure and Functio. *Crit. Rev. Biochem. Mol. Biol.* **1989**, *24*, 69–99. [CrossRef]
16. Chrysina, E.D.; Chajistamatiou, A.; Chegkazi, M. From Structure—Based to Knowledge—Based Drug Design Through X-Ray Protein Crystallography: Sketching Glycogen Phosphorylase Binding Sites. *Curr. Med. Chem.* **2011**, *18*, 2620–2629. [CrossRef]
17. Chehardoli, G.; Bahmani, A. Synthetic Strategies, SAR Studies, and Computer Modeling of Indole 2 and 3-Carboxamides as the Strong Enzyme Inhibitors: A Review. *Mol. Divers.* **2021**, *25*, 535–550. [CrossRef] [PubMed]
18. Minadakis, M.P.; Mavreas, K.F.; Neofytos, D.D.; Paschou, M.; Kogkaki, A.; Athanasiou, V.; Mamais, M.; Veclani, D.; Iatrou, H.; Venturini, A.; et al. A Glucose-Based Molecular Rotor Inhibitor of Glycogen Phosphorylase as a Probe of Cellular Enzymatic Function. *Org. Biomol. Chem.* **2022**, *20*, 2407–2423. [CrossRef] [PubMed]
19. Klinov, S.V.; Chebotareva, N.A.; Lissovskaya, N.P.; Davidov, D.R.; Kurganov, B.I. The interaction of muscle glycogen phosphorylase b with glycogen. *Biochim. Biophys. Acta Protein Struct. Mol. Enzymol.* **1982**, *709*, 91–98. [CrossRef] [PubMed]
20. Karayianni, M.; Pispas, S. Complexation of Stimuli-Responsive Star-like Amphiphilic Block Polyelectrolyte Micelles with Lysozyme. *Soft Matter* **2012**, *8*, 8758–8769. [CrossRef]
21. Karayianni, M.; Koufi, D.; Pispas, S. Development of Double Hydrophilic Block Copolymer/Porphyrin Polyion Complex Micelles towards Photofunctional Nanoparticles. *Polymers* **2022**, *14*, 5186. [CrossRef]
22. Appleman, M.M.; Yunis, A.A.; Krebs, E.G.; Fischer, E.H. Comparative Studies on Glycogen Phosphorylase. *J. Biol. Chem.* **1963**, *238*, 1358–1361. [CrossRef] [PubMed]
23. De Lange, R.J.; Kemp, R.G.; Riley, W.D.; Cooper, R.A.; Krebs, E.G. Activation of Skeletal Muscle Phosphorylase Kinase by Adenosine Triphosphate and Adenosine 3′,5′-Monophosphate. *J. Biol. Chem.* **1968**, *243*, 2200–2208. [CrossRef] [PubMed]
24. Einstein, A. Über Einen Die Erzeugung Und Verwandlung Des Lichtes Betreffenden Heuristischen Gesichtspunkt. *Ann. Phys.* **1905**, *322*, 132–148. [CrossRef]
25. Kissa, E. Particle Characterization. In *Dispersions*; Routledge: London, UK, 2017; Volume 81, pp. 8–46.
26. Huglin, M.B. *Light Scattering from Polymer Solutions*; Academic Press: London, UK; New York, NY, USA, 1972; ISBN 0123610508.
27. Ioan, C.E.; Aberle, T.; Burchard, W. Solution Properties of Glycogen. 1. Dilute Solutions. *Macromolecules* **1999**, *32*, 7444–7453. [CrossRef]
28. Ioan, C.E.; Aberle, T.; Burchard, W. Solution Properties of Glycogen. 2. Semidilute Solutions. *Macromolecules* **1999**, *32*, 8655–8662. [CrossRef]
29. ThermoFisher Scientific. The Molecular Probes® Handbook—Introduction to Fluorescence Techniques. In *The Molecular Probes^{TM} Handbook—A Guide to Fluorescent Probes and Labeling Technologies*, 11th ed.; Johnson, I., Spence, M.T.Z., Eds.; Life Technologies: Carlsbad, CA, USA, 2010; pp. 3–9.
30. Zhang, S.Z.; Zhao, F.L.; Li, K.A.; Tong, S.Y. Determination of Glycogen by Rayleigh Light Scattering. *Anal. Chim. Acta* **2001**, *431*, 133–139. [CrossRef]
31. Morris, G.A.; Ang, S.; Hill, S.E.; Lewis, S.; Scha, B.; Nobbmann, U.; Harding, S.E. Molar mass and solution conformation of branched α(1→4), α(1→6) Glucans. Part I: Glycogens in water. *Carbohydr. Polym.* **2008**, *71*, 101–108. [CrossRef]
32. Rolland-Sabaté, A.; Mendez-Montealvo, M.G.; Colonna, P.; Planchot, V. Online Determination of Structural Properties and Observation of Deviations from Power Law Behavior. *Biomacromolecules* **2008**, *9*, 1719–1730. [CrossRef]
33. Sullivan, M.A.; O'Connor, M.J.; Umana, F.; Roura, E.; Jack, K.; Stapleton, D.I.; Gilbert, R.G. Molecular Insights into Glycogen α-Particle Formation. *Biomacromolecules* **2012**, *13*, 3805–3813. [CrossRef]
34. Fernandez, C.; Rojas, C.C.; Nilsson, L. Size, Structure and Scaling Relationships in Glycogen from Various Sources Investigated with Asymmetrical Flow Field-Flow Fractionation and ^{1}H NMR. *Int. J. Biol. Macromol.* **2011**, *49*, 458–465. [CrossRef]
35. Filippov, S.K.; Sedlacek, O.; Bogomolova, A.; Vetrik, M.; Jirak, D.; Kovar, J.; Kucka, J.; Bals, S.; Turner, S.; Stepanek, P.; et al. Glycogen as a Biodegradable Construction Nanomaterial for in Vivo Use. *Macromol. Biosci.* **2012**, *12*, 1731–1738. [CrossRef] [PubMed]
36. Wojnilowicz, M.; Besford, Q.A.; Wu, Y.; Loh, X.J.; Braunger, J.A.; Glab, A.; Cortez-Jugo, C.; Caruso, F.; Cavalieri, F. Glycogen-Nucleic Acid Constructs for Gene Silencing in Multicellular Tumor Spheroids. *Biomaterials* **2018**, *176*, 34–49. [CrossRef]
37. Ghisaidoobe, A.B.T.; Chung, S.J. Intrinsic Tryptophan Fluorescence in the Detection and Analysis of Proteins: A Focus on Förster Resonance Energy Transfer Techniques. *Int. J. Mol. Sci.* **2014**, *15*, 22518–22538. [CrossRef] [PubMed]

38. Smeller, L.; Meersman, F.; Heremans, K. Refolding Studies Using Pressure: The Folding Landscape of Lysozyme in the Pressure-Temperature Plane. *Biochim. Biophys. Acta—Proteins Proteom.* **2006**, *1764*, 497–505. [CrossRef]
39. Nielsen, M.M.; Andersen, K.K.; Westh, P.; Otzen, D.E. Unfolding of β-Sheet Proteins in SDS. *Biophys. J.* **2007**, *92*, 3674–3685. [CrossRef] [PubMed]